# Intelligent multimodal medical image fusion with deep guided filtering

B. Rajalingam[1] · Fadi Al-Turjman[2] · R. Santhoshkumar[1] · M. Rajesh[3]

## Abstract

Medical image fusion is a synthesis of visual information present in any number of medical imaging inputs into a single fused image without any distortion or loss of detail. It enhances image quality by retaining specific features to improve the clinical applicability of medical imaging for treatment and evaluation of medical conditions. A big challenge in the processing of medical images is to incorporate the pathological features of the complement into one image. The fused image presents various challenges, such as existence of fusion artifacts, hardness of the base, comparison of medical image input, and computational cost. The techniques of hybrid multimodal medical image fusion (HMMIF) have been designed for pathologic studies, such as neurocysticercosis, degenerative and neoplastic diseases. Two domain algorithms based on HMMIF techniques have been developed in this research for various medical image fusion applications for MRI-SPECT, MRI-PET, and MRI-CT. NSCT is initially used in the proposed method to decompose the input images which give components of low and high frequency. The average fusion rule applies to NSCT components with low frequency. The NSCT high frequency components are fused by the law of full fusion. NSCTs high frequency is handled with directed image filtration scheme. The fused picture is obtained by taking inverse transformations from all frequency bands with the coefficients obtained from them. The methods suggested are contrasted with traditional approaches in the state of the art. Experimentation proves that the methods suggested are superior in terms of both qualitative and quantitative assessment. The fused images using proposed algorithms provide information useful for visualizing and understanding the diseases to the best of both sources' modality.

## 1 Introduction

Several changes have been seen in clinical applications with advancement in technology and there has been a huge Increase of the number of images modality. The imaging technique used for medical purposes offers specialized information which is not otherwise accessible. Doctors need details from more than one approach to diagnose an illness properly [1, 2]. CT scans provide details on dense bone structures for accurate radiation, dose assessment, but do not offer any insight into internal organs. The MRI images demonstrate the hard tissue contrast, but lack bone information. Radiologists; therefore, require the fusion of two or more modalities Because of the inability of one single image to have all the details. By image fusion, using many techniques, better disease analyzes can be given by integrating information from more than one modality. CT and MRI image fusion allow for combined Representation of the connective tissue information provided by the MRI image and the CT image of the vertebral anatomy, which makes doctors understand the disease as well as provide decent healthcare. Image fusion efforts to integrate the necessary information from both images into one image, and care should be taken when fusing to avoid adding any artifacts to the image [27–2]. Spatial image fusion, transformations, neural networks and directed image filtering may be implemented. PCA, DWT,

✉ M. Rajesh
  rajesmano@gmail.com

1 Department of CSE, Priyadarshini College of Engineering and Technology, Nellore, Andhra Pradesh, India

2 Artificial Intelligence Engineering Department, Research Centre for AI and IoT, Near East University, Mersin 10, Nicosia, Turkey

3 Department of Computer Science and Engineering, Sanjivani College of Engineering, Kopargaon, India

CVT, NSST, and GIF are the basic traditional fusion methods. However, these methods are not very successful in fusing specific source image information and leading to certain objects.

In the recent years, the study of pixel level image fusion has lasted for more than 30 years, during which around 1 k of related scientific papers have been published. Currently deep learning (DL) has gained many breakthroughs in various computer vision and image processing problems, such as classification, segmentation, super-resolution, etc. In the field of image fusion, the study based on deep learning has also become an active topic in the last three years. A variety of DL-based image fusion methods have been proposed for digital photography (e.g., multifocus image fusion, multi-exposure image fusion), multimodality imaging (e.g., medical image fusion, infrared/visible image fusion). In this paper, this issue is addressed from another viewpoint to overcome the difficulty in designing robust activity level measurements and weight assignment strategies. Specifically, a convolutional neural network (CNN) is trained to encode a direct mapping from input medical images to the weight map. In this way, the activity level measurement and weight assignment can be jointly achieved in an "optimal" manner via learning network parameters. Considering the different imaging modalities of multimodal medical images, we adopt a multiscale approach via image pyramids to make fusion process more consistent with human visual perception. In addition, a local similarity-based strategy is applied to adaptively adjust the fusion mode for the decomposed coefficients of input multimodal medical images [4].

Therefore, methods of hybrid fusion seek to solve those shortcomings of conventional methods. Owing to the appealing advantages in the medical decision-making team, the issue of multimodal medical image fusion has provided focused work in the recent years [5].

## 2 Literature survey

James et al. [6] lists the methods factually and describes the specific technical challenges facing the medical image fusion field. The process for fusing medical images using DTCWT and SOFM was proposed by Karthikeyan et al. [7]. Gupta [8] suggested the integration of medical images with CT and MR in the NSST domain using the adaptive neural spiking technique. Daniel suggested a homomorphic fusion of wavelets called optimum homomorphic fusion of wavelets using hybrid GWO algorithm. Daniel et al. [9] suggested an optimum spectrum mask fusion using traditional GWO algorithms for MIF. S.H. For both CT and MRI medical images, Bhadauria et al. [10] proposed a noise reduction approach which fuses the images by processing them via CVT. Hermessi et al. [11] proposed a CNN-based fusion process

for CT and MR medical images in the ST. Shahdoosti et al. [12] proposed the MMIF tetrolet transform. Heba et al. [13] Analyzes several clinical image fusion techniques and discusses the most important strengths and limitations of these techniques in developing hybrid techniques that improve the consistency of the combined image. Xi et al. [14] suggested an MMIF algorithm for clinical condition research, combined with sparse representation and PCNN. Xia et al. [15] suggested a novel fusion scheme for MMI using both the multiscale transformation features as well as DCNN. El-Hoseny et al. [16] discusses some of the MIF techniques to improve the hybrid fusion algorithm to enhance the fused image quality. Chavan et al. [17] suggested transforming NSxRW-based image fusion used for NCC review and post-treatment inspection. Sharma, et al. proposed image fusion algorithm based on NSST with simplified PCNN model. Sreeja et al. [18] suggested a fusion algorithm which would fuse the diagnostic image and improve the image quality of the fusion. Xua in [19] proposed the medical image fusion DFRWT process. Liu et al. [20] suggested a tensor structure and NSST to extract geometric functionality and apply a unified optimization model for image fusion. Liu et al. [21] suggested a NSST-based fusion algorithm that exploits decomposition based on moving frames. Liu et al. [22] proposed the medical image fusion method based on the convolutional neural networks (CNNs). Liu et al. [23] proposed the new multifocus image fusion method based on the deep learning approach, aiming to learn a direct mapping between source images and focus map. A deep convolutional neural network (CNN) trained by high-quality image patches and their blurred versions is adopted to encode the mapping. Liu et al. [24] presented the survey paper on a systematic review of the DL-based pixel-level image fusion literature. This paper specifically summarizes the main difficulties that exist in conventional image fusion research and discusses the advantages that DL can offer to address each of these problems. Rajalingam et al. [4] proposed an efficient multimodal medical image fusion approach based on the deep learning neural networks (CNN) for fusion process. Du and Gao [25] proposed a new all CNN (ACNN)-based multifocus image fusion method in spatial domain. The main idea is that the max-pooling of CNN is replaced by a convolution layer, the residuals are propagated backwards by gradient descent, and the training parameters of the individual layers of the CNN are updated layer by layer.

## 3 Proposed hybrid image fusion algorithm (NSCT-GIF)

Fusion is performed using the NSCT and guided filtering shown in Fig. 1 on recorded input medical images X and Y.

**Fig. 1** Block diagram for the proposed hybrid fusion algorithm (NSCT—GIF)
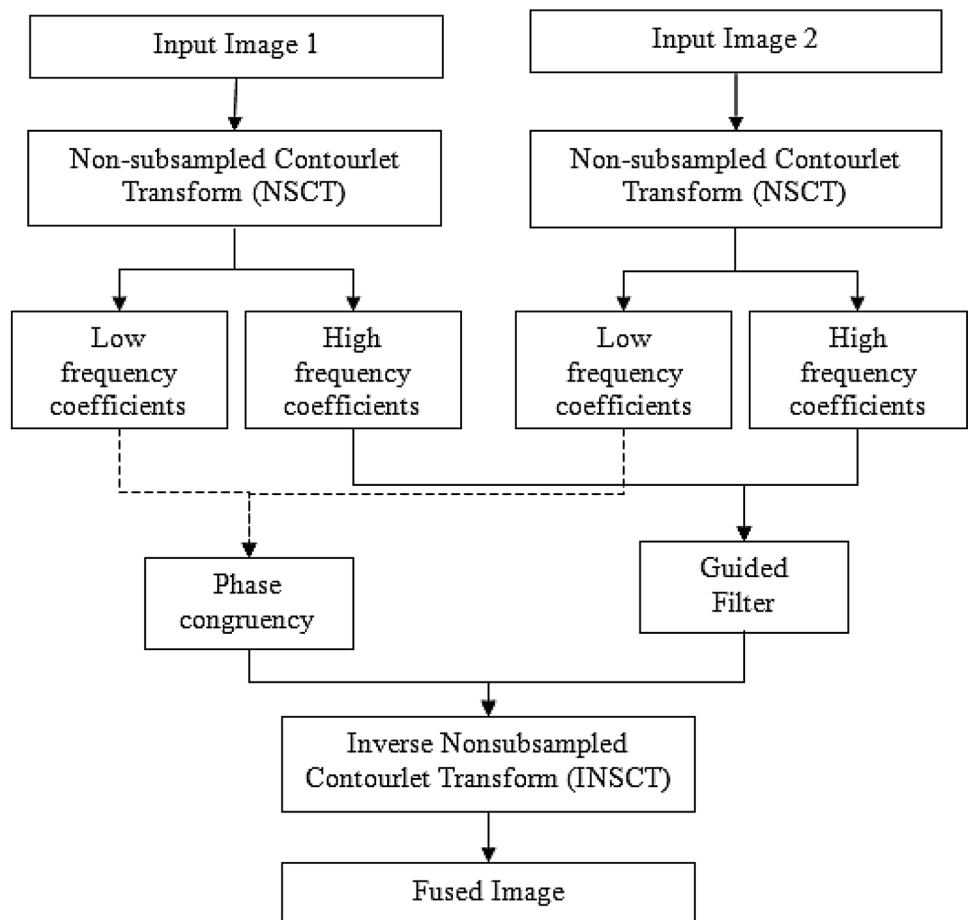


## 3.1 Procedural steps for the hybrid fusion algorithm (NSCT—GIF)

*Step 1* 1: Read the two medical images X and Y for data.

*Step 2* 2: Decomposition of images from source.

Decompose the source modalities using NSCT. Input modalities is decomposed into low and high frequency images at each level and direction, $\theta$, i.e., $A : \{C_L^X \cdot C_L^X\}$, $B : \{C_L^Y \cdot C_L^Y\}\}$, Here $C_L$ represents images of low frequency and high frequency at the stage $L$ and orientation. In the process, the degree of decomposition is 3 as described in [26].

*Step 3* Coefficients of low frequency fusion.

$$P = \frac{\sum W^\circ x, y \left[ A_{x,y}^\circ \right] \left( \cos \left( \theta_{x,y}^\circ \right) \right)}{\sum_n A_{x,y} + \in}. \tag{1}$$

$$C_L^F(a,b) = C_L^X(a,b), \text{ if } P_{cl}^X(a,b) > P_{cl}^Y(a,b) \tag{2}$$

$$C_L^F(a,b) = C_L^Y(a, yb), \text{ if } P^Y(a,b) > P_{cl}^Y(a,b) \tag{3}$$

$$C_L^F(a,b) = (C_L^Y(a,b) + C_L^X(a,b))/2, \text{ if } P_{cl}^X(a,b) = P_{cl}^Y(a,b). \tag{4}$$

*Step 4* High frequency fusion coefficients.

$$Q_i = \frac{1}{|w|} \sum_{i \in wk} (a_k I_i + b_k) \tag{5}$$

High frequency coefficient is the guiding feature in this method $X\, C_L^X$ then input image is the coefficient of the high frequency signal $Y\, C_L^Y$ for each level the output image is generated. All the higher frequencies images are then fused to produce a simple average $C_L^F$, $Q_i$—linear alteration of guideline picture.

*Step 5* Inverse NSCT exists on the $C_L^F$ to get a photo fused F.

## 3.2 NSCT

The NSCT is based on the Contourlet Transform principle that produces better outcomes in the visualization of geometrical images. The Contourlet Transform is a category of transition, as it involves down-samplers as well as up-samplers in the Laplacian pyramid levels as well as the dimensional
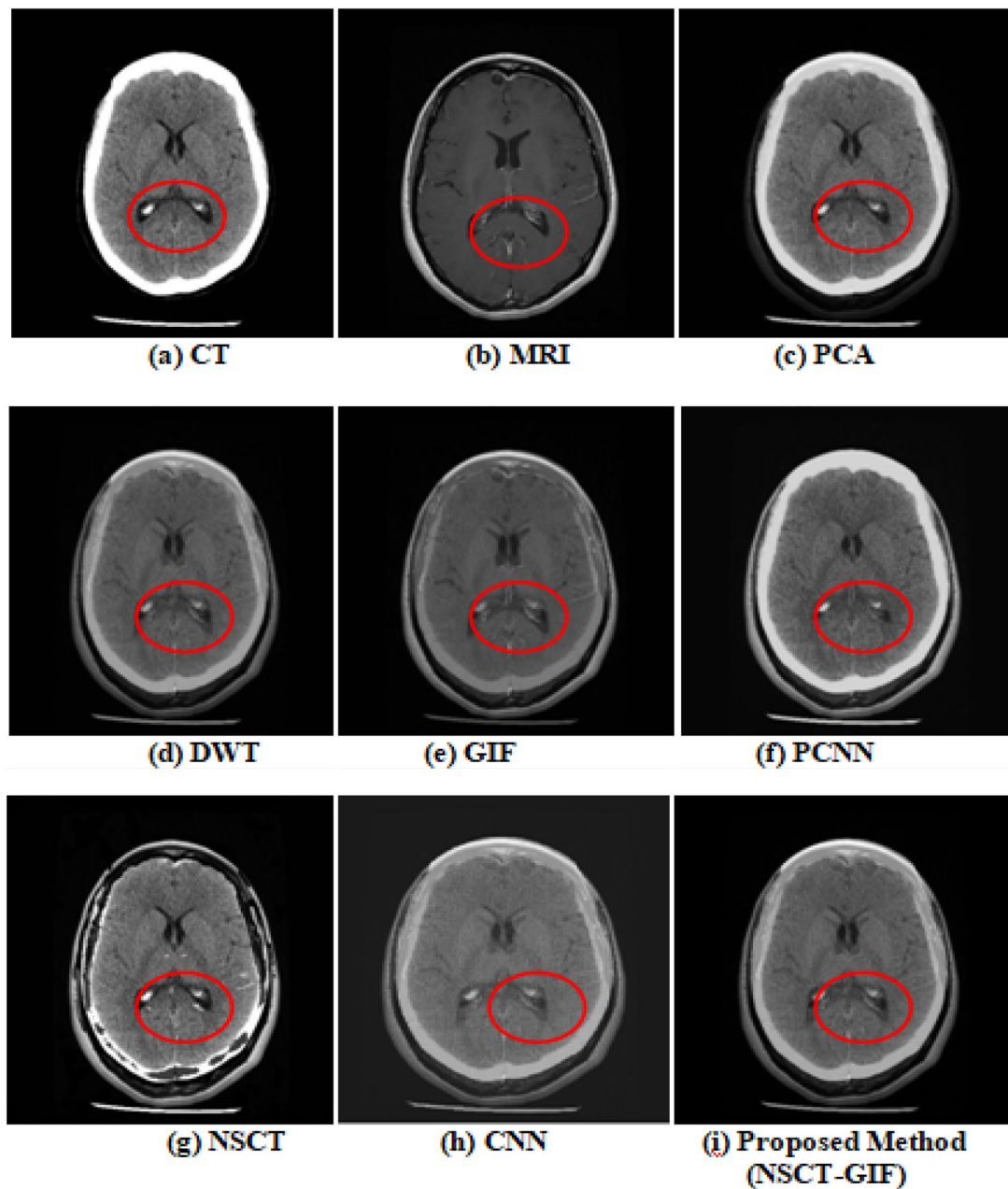
**Fig. 2** Experimental results for neurocysticercosis disease affected images (set 1)

bank filter. NSCT is an invariant, multiscale, and multidirectional shift conversion whose integration is very complex. This is accessed via the NSPFB and NSDFB [27].

### 3.3 Phase congruency

It is a contrasting invariant texture analysis method based on a local energy model, which follows the concept that significant features can be found in a picture in which the Fourier coefficients are up to the limit. It is also insensitive to map
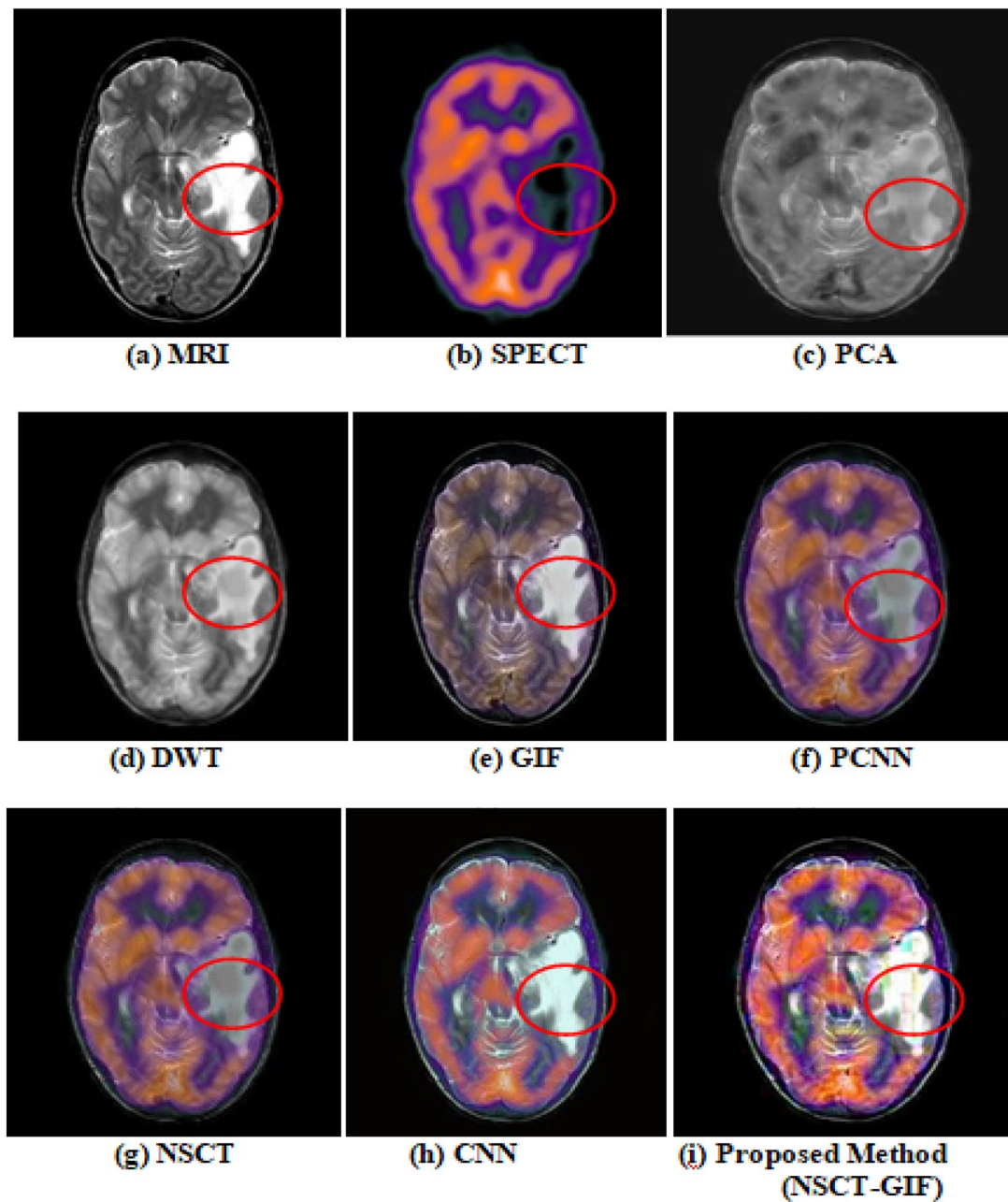
**Fig. 3** Experimental results for metastatic bronchogenic carcinoma disease affected images (set 2)

specific pixel pressure. It is insensitive to cause changes in illumination and contrast that makes it ideal for the use in fusion of multimodal medical images. It is a good feature for fusing clinical multimodal data. In the proposed method, it is then used as a fusion rule for the low frequency components (NSCT-GIF) [28, 26].

### 3.4 Guided image filtering (GIF)

$$Q_i = a_k I_i + b_k \forall i \in w_k \tag{6}$$

$$a_k = \frac{1}{W} \frac{\sum_{i \in w_k} I_I t_i - u_k E[t_k]}{\sigma_k^2 + \in} \tag{7}$$
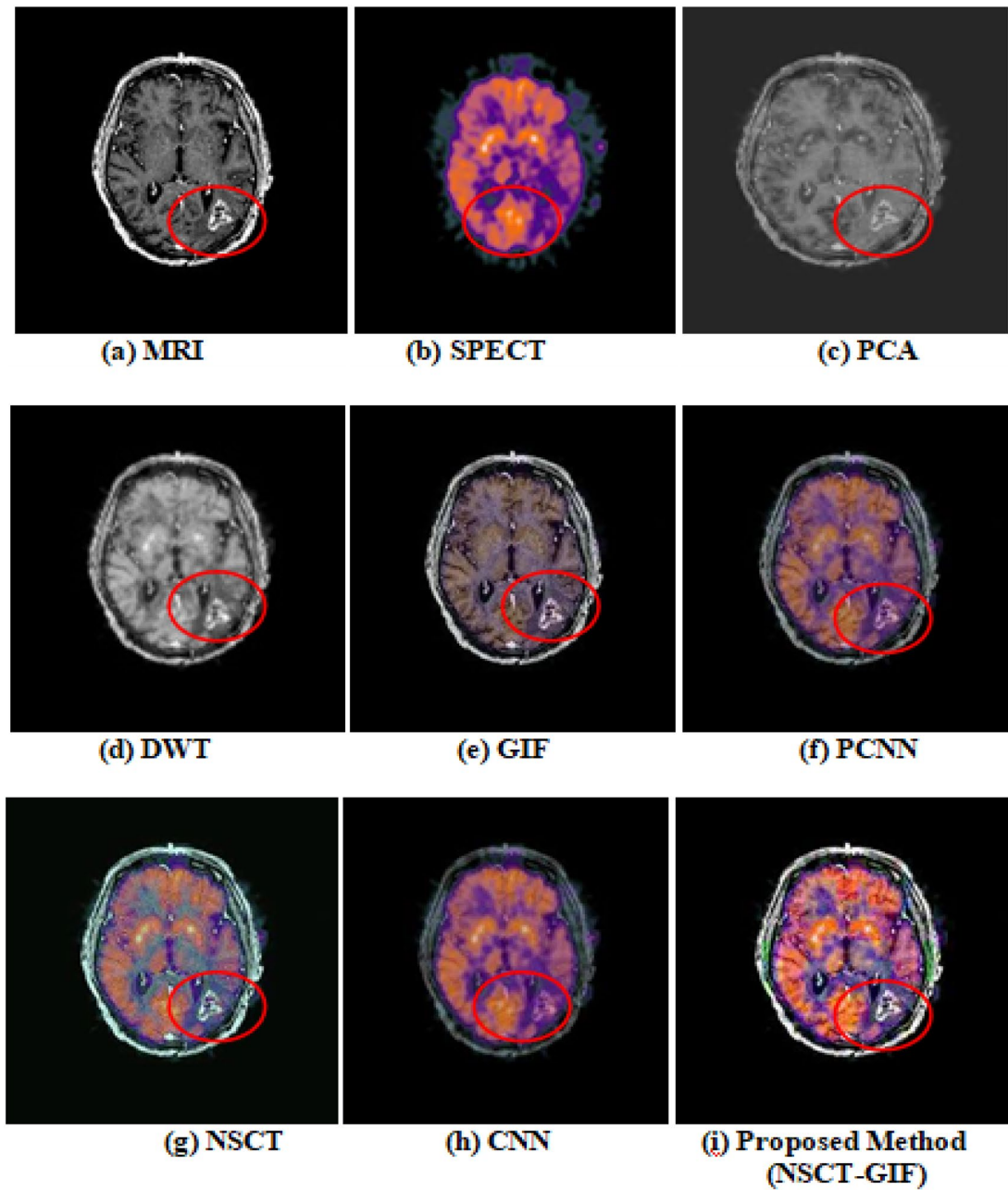
**Fig. 4** Experimental results for astrocytoma disease affected images (set 3)

$$b_k = E(t_k) - a_k u_k \qquad (8)$$

where $a_k$ and $b_k$ are the coefficients unchanged in $w_k$. The coefficients $a_k$ and $b_k$ can be found using Eqs. (7) and (8). $E(t_k)$ returns the mean image data in the window $w_k$. The mean and the difference of the window feature $w_k$ are represented by $u_k$ and $\sigma_k^2$. Driven image filter has been used extensively for image fusion and provides good results for combining multimodal clinical data [3].
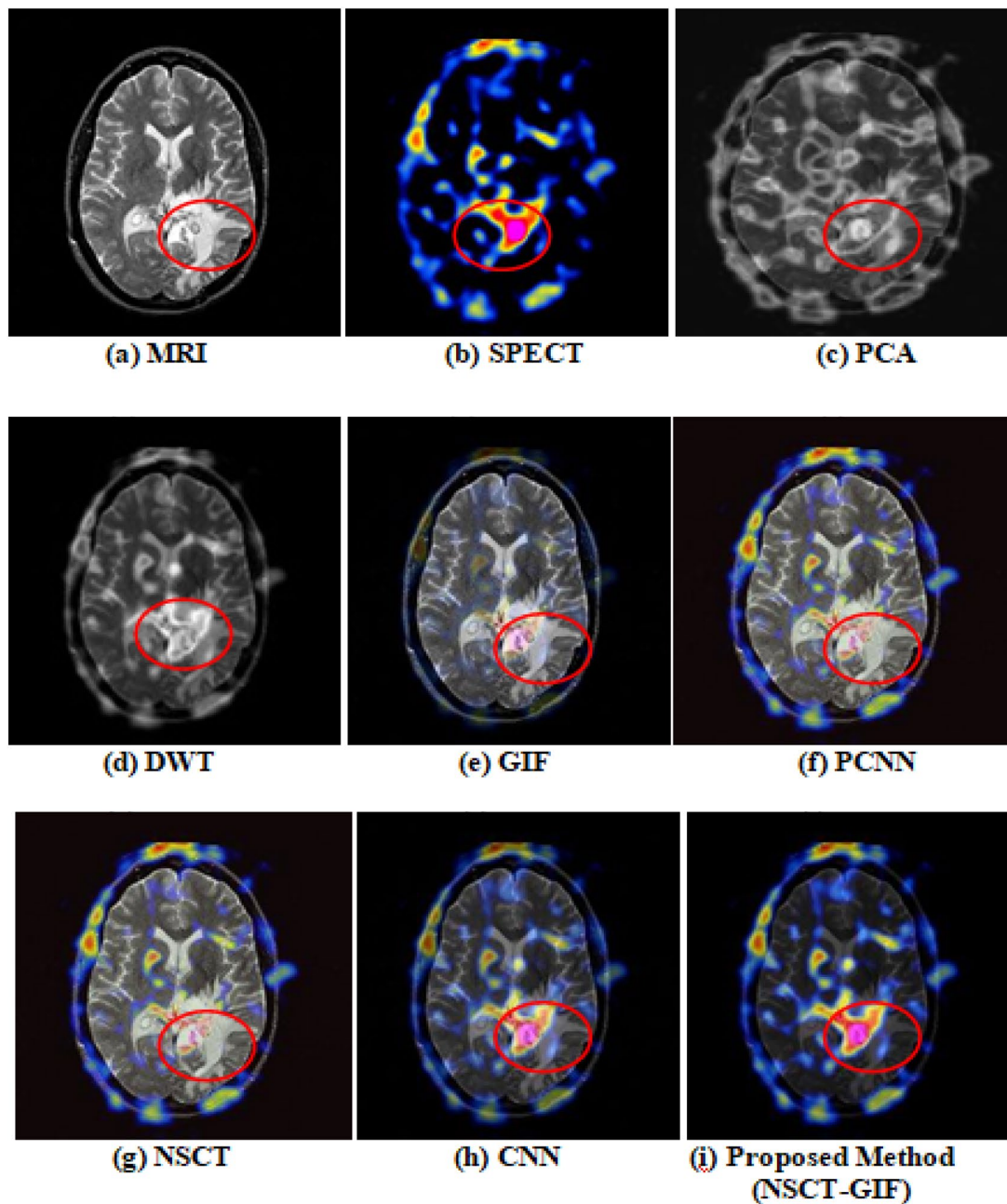
**Fig. 5** Experimental results for anaplastic astrocytoma affected images (set 4)

## 4 Experimental outcomes and discussion

The proposed HMMIF methodology is evaluated for clinicians diagnosed with neurocysticercosis, incurable, and neoplastic disorders on pilot study sets incorporating CT and MRI, MRI and PET, MRI and SPECT of the brain. The mixture of each pair of input images of both CT and MRI sketches, MRI and PET sketches, and MRI and SPECT slices was chosen from the same individual based on the clinical and operational comparisons. The analysis results of the proposed composite image fusion strategies and other current strategies are shown in Figs. 2, 3, 4, 5, 6, and 7,
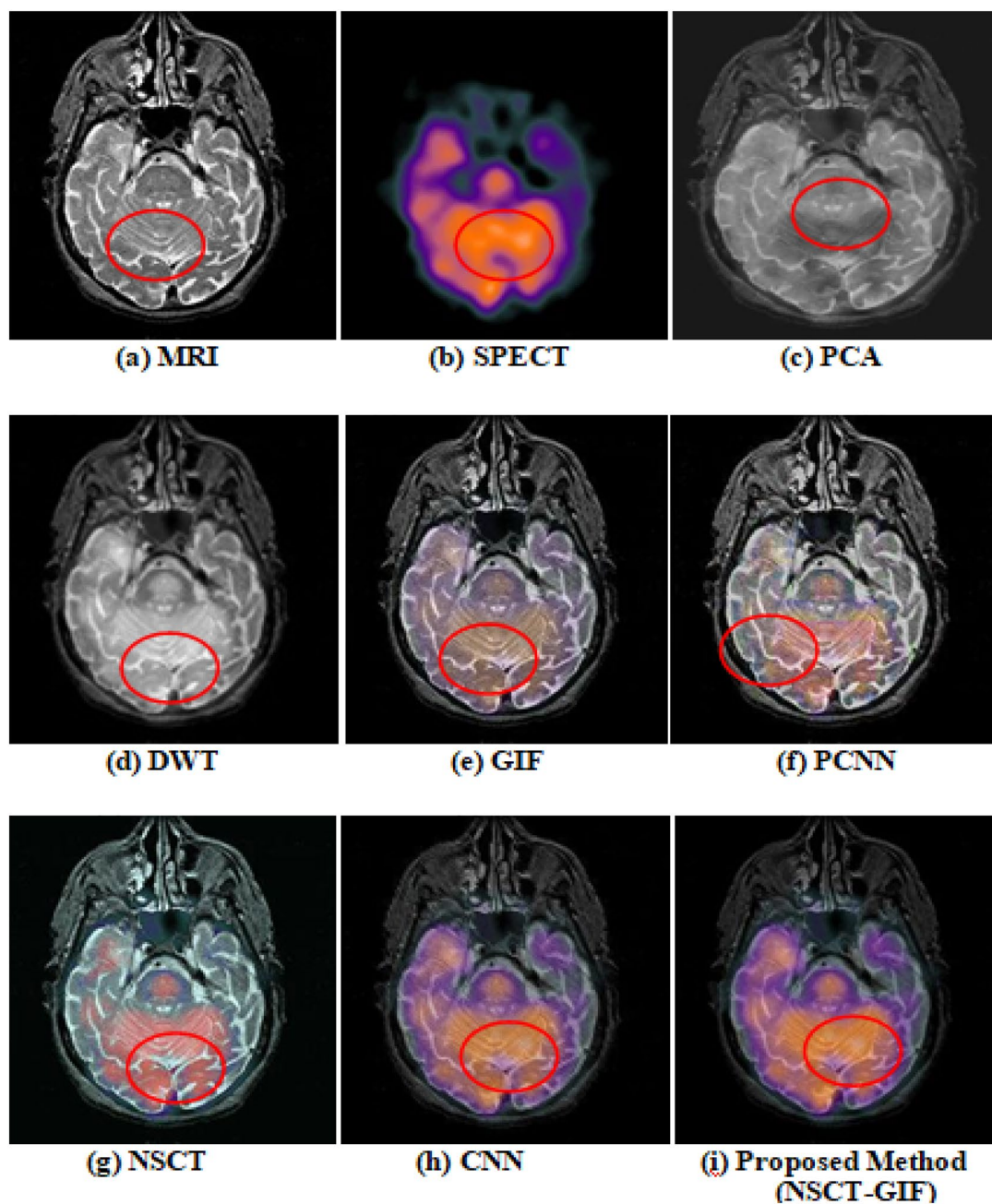
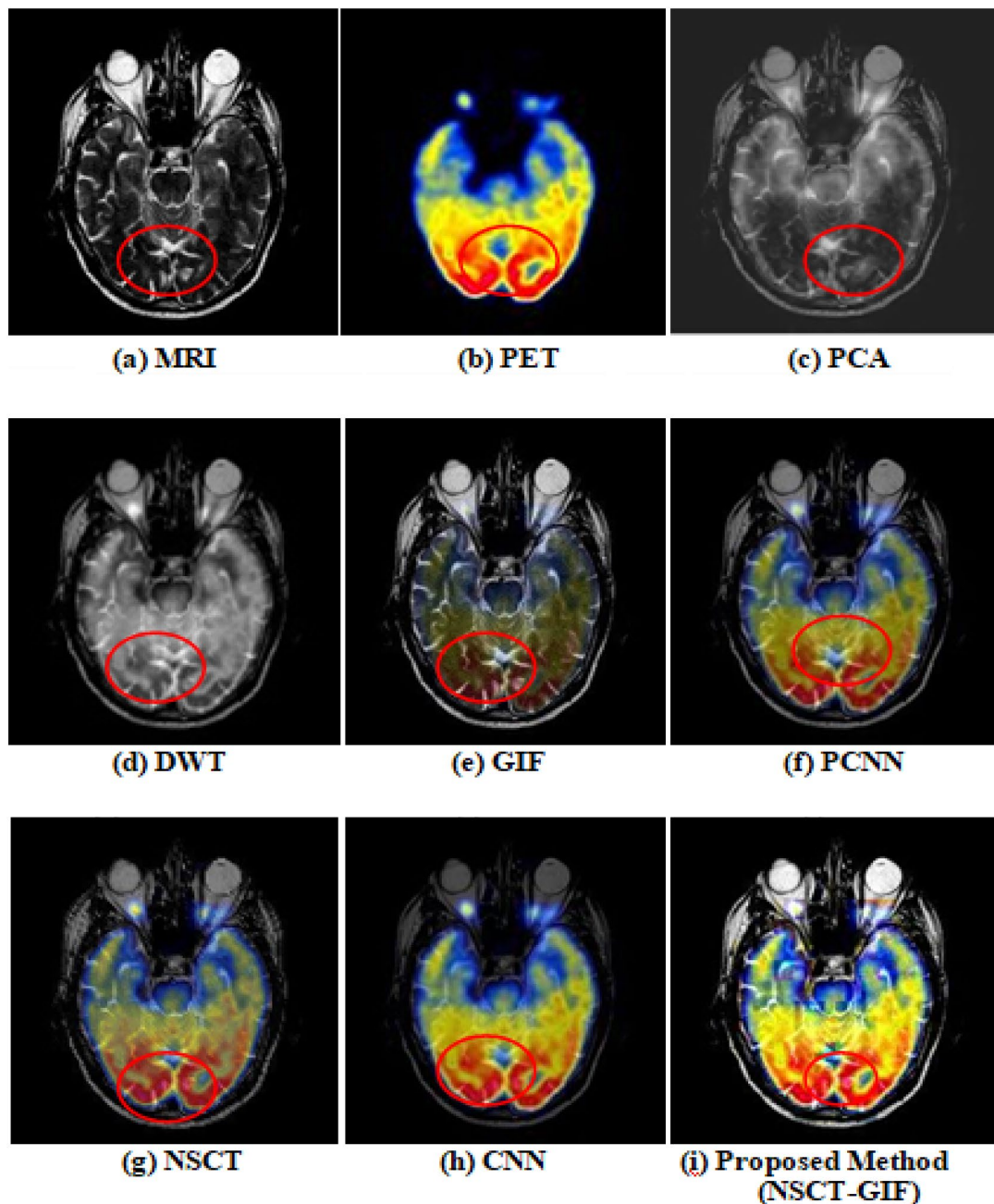**Fig. 6** Experimental results for Alzheimer's affected images (set 5)

which allow the output of the proposed fusion strategies to be compared and analyzed. The processed multimodality medical input images are gathered from Harvard medical school [30] and radiopedia.org [31] medical image online database. The size of the image is $256 \times 256$ for execution process.

For the image fusion six separate sets of CT/MRI, MRI/ PET, and MRI/SPECT images will be taken. The set 1 of input images reflects the diagnostic images of the patient

harmed by neurocysticercosis disease taken from CT and MRI scanners, respectively.

The set 2 of input images reflects the metastatic bronchogenic carcinoma disease caused by brain images in the MRI/SPECT combination. The 3 and 4 sets of input images reflect the affected brain images of astrocytoma and anaplastic astrocytoma disease in the MRI/SPECT combination, respectively. The 5 and 6 sets of input images show the affected brain images of the Alzheimer and mild Alzheimer

**Fig. 7** Experimental results for mild Alzheimer's disease affected images (set 6)

disease in conjunction with MRI/SPECT and MRI/PET, respectively.

Using the mixture of hybrid algorithm (NSCT—GIF) the fusion results in the same input images using PCA, DWT, GIF, PCNN, NSCT, CNN, and proposed hybrid technique (NSCT-GIF). The fusion outcome of the proposed hybrid methodology delivers better efficiency in both theoretical and practical analysis, out of all conventional fusion strategies.

The comprehensive analysis of performance measures for traditional and theoretical hybrid fusion strategies such as fusion component, IQI, mSSIM, cross entropy, EQM, MI, PSNR, and standard deviation are shown in Tables 1 and 2. The target for the performance metrics values of the fusion factor should be the highest value for an effective image fusion methodology, the highest value should be IQI, mSSIM, EQM, and cross entropy, and the value closest to '1' should also be proclaimed as a higher quality for the fused output image.

**Table 1** Performance metrics comparative analysis for different fusion methods (set 1, set 2, and set 3)

| Study set | Algorithm | Metrics | | | | | | | |
|---|---|---|---|---|---|---|---|---|---|
| | | FusFac | IQI | mSSIM | $CE_n$ | EQM | MI | PSNR | STD |
| Set 1 | PCA | 1.576 | 0.429 | 0.423 | 1.263 | 0.579 | 2.304 | 35.38 | 34.58 |
| | DWT | 2.389 | 0.441 | 0.438 | 1.378 | 0.584 | 2.505 | 37.08 | 36.20 |
| | GIF | 2.479 | 0.553 | 0.522 | 1.359 | 0.596 | 2.805 | 39.64 | 40.63 |
| | PCNN | 2.171 | 0.586 | 0.550 | 1.295 | 0.579 | 2.603 | 38.30 | 38.40 |
| | NSCT | 3.145 | 0.603 | 0.593 | 1.582 | 0.633 | 2.905 | 44.69 | 43.55 |
| | CNN | 4.072 | 0.908 | 0.890 | 0.773 | 0.8945 | 3.34 | 54.70 | 47.4 |
| | Proposed method (NSCT-GIF) | 4.191 | 0.941 | 0.924 | 0.672 | 0.9301 | 3.501 | 55.06 | 49.5 |
| Set 2 | PCA | 1.154 | 0.462 | 0.423 | 1.511 | 0.451 | 1.962 | 29.05 | 32.10 |
| | DWT | 2.265 | 0.558 | 0.548 | 1.481 | 0.508 | 2.049 | 32.39 | 34.50 |
| | GIF | 2.412 | 0.542 | 0.595 | 1.322 | 0.549 | 2.402 | 35.55 | 37.20 |
| | PCNN | 2.531 | 0.528 | 0.575 | 1.208 | 0.592 | 2.603 | 37.40 | 35.07 |
| | NSCT | 3.612 | 0.701 | 0.670 | 0.969 | 0.722 | 2.952 | 39.58 | 38.81 |
| | CNN | 4.02 | 0.92 | 0.9392 | 0.5674 | 0.8987 | 3.502 | 45.72 | 42.1 |
| | Proposed method (NSCT-GIF) | 4.142 | 0.94 | 0.9412 | 0.529 | 0.9301 | 3.65 | 46.62 | 44.1 |
| Set 3 | PCA | 1.201 | 0.487 | 0.451 | 2.190 | 0.437 | 2.506 | 32.68 | 24.45 |
| | DWT | 1.391 | 0.521 | 0.558 | 1.521 | 0.429 | 2.740 | 33.76 | 27.06 |
| | GIF | 2.412 | 0.594 | 0.581 | 1.592 | 0.442 | 2.904 | 38.56 | 29.10 |
| | PCNN | 2.741 | 0.625 | 0.591 | 1.661 | 0.458 | 2.620 | 35.80 | 28.31 |
| | NSCT | 2.662 | 0.682 | 0.693 | 1.245 | 0.561 | 2.902 | 39.67 | 29.45 |
| | CNN | 4.1213 | 0.968 | 0.9364 | 0.5707 | 0.9482 | 3.306 | 43.65 | 32.43 |
| | Proposed method (NSCT-GIF) | 4.3044 | 0.997 | 0.9852 | 0.5215 | 0.962 | 3.502 | 45.68 | 35.76 |

**Table 2** Performance metrics comparative analysis for different fusion methods (set 4, set 5, and set 6)

| Study set | Algorithm | Metrics | | | | | | | |
|---|---|---|---|---|---|---|---|---|---|
| | | FusFac | IQI | mSSIM | $CE_n$ | EQM | MI | PSNR | STD |
| Set 4 | PCA | 1.216 | 0.433 | 0.436 | 2.527 | 0.476 | 2.502 | 28.60 | 39.65 |
| | DWT | 1.519 | 0.529 | 0.472 | 2.075 | 0.561 | 2.822 | 29.45 | 42.53 |
| | GIF | 1.741 | 0.611 | 0.548 | 1.822 | 0.609 | 3.035 | 32.56 | 45.40 |
| | PCNN | 1.621 | 0.652 | 0.589 | 1.731 | 0.643 | 2.869 | 35.32 | 50.20 |
| | NSCT | 1.799 | 0.802 | 0.645 | 1.203 | 0.699 | 3.056 | 39.78 | 65.61 |
| | CNN | 2.9515 | 0.988 | 0.9295 | 0.9511 | 0.9048 | 3.478 | 43.8 | 85.2 |
| | Proposed method (NSCT-GIF) | 3.0163 | 0.972 | 0.9545 | 0.9463 | 0.9153 | 3.55 | 45.87 | 86.08 |
| Set 5 | PCA | 1.523 | 0.414 | 0.450 | 1.487 | 0.573 | 3.256 | 34.78 | 23.47 |
| | DWT | 1.838 | 0.528 | 0.520 | 1.463 | 0.585 | 3.467 | 36.40 | 24.04 |
| | GIF | 2.152 | 0.574 | 0.602 | 1.338 | 0.619 | 4.230 | 43.01 | 26.34 |
| | PCNN | 2.051 | 0.602 | 0.646 | 1.452 | 0.597 | 4.056 | 40.23 | 28.76 |
| | NSCT | 2.572 | 0.664 | 0.696 | 1.012 | 0.676 | 4.490 | 45.30 | 34.56 |
| | CNN | 3.9375 | 0.893 | 0.8505 | 0.5289 | 0.8647 | 4.845 | 50.2 | 38.56 |
| | Proposed method (NSCT-GIF) | 3.983 | 0.932 | 0.9056 | 0.451 | 0.9201 | 4.992 | 52.3 | 39.06 |
| Set 6 | PCA | 1.276 | 0.567 | 0.529 | 1.873 | 0.479 | 3.256 | 30.56 | 28.56 |
| | DWT | 1.376 | 0.573 | 0.548 | 1.769 | 0.517 | 3.467 | 32.58 | 32.10 |
| | GIF | 1.469 | 0.619 | 0.629 | 0.984 | 0.543 | 3.967 | 34.56 | 34.45 |
| | PCNN | 1.652 | 0.596 | 0.605 | 0.678 | 0.597 | 3.734 | 33.30 | 32.03 |
| | NSCT | 1.678 | 0.769 | 0.695 | 0.657 | 0.669 | 3.984 | 38.40 | 36.42 |
| | CNN | 2.5589 | 0.902 | 0.8984 | 0.5846 | 0.9098 | 4.46 | 47.46 | 38.4 |
| | Proposed method (NSCT-GIF) | 2.9014 | 0.926 | 0.9804 | 0.5604 | 0.9334 | 4.502 | 48.4 | 39.4 |
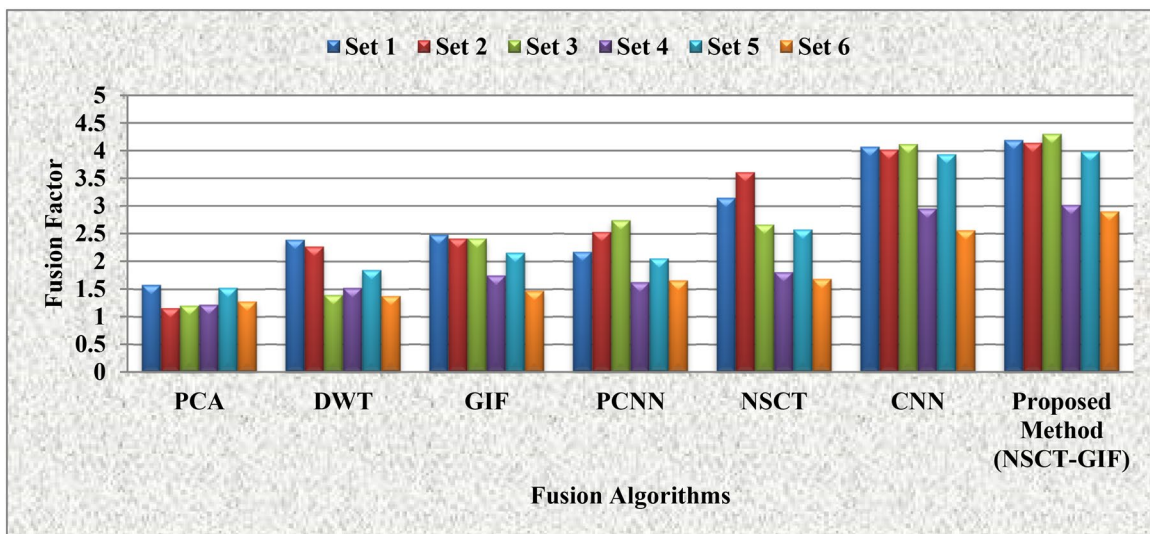
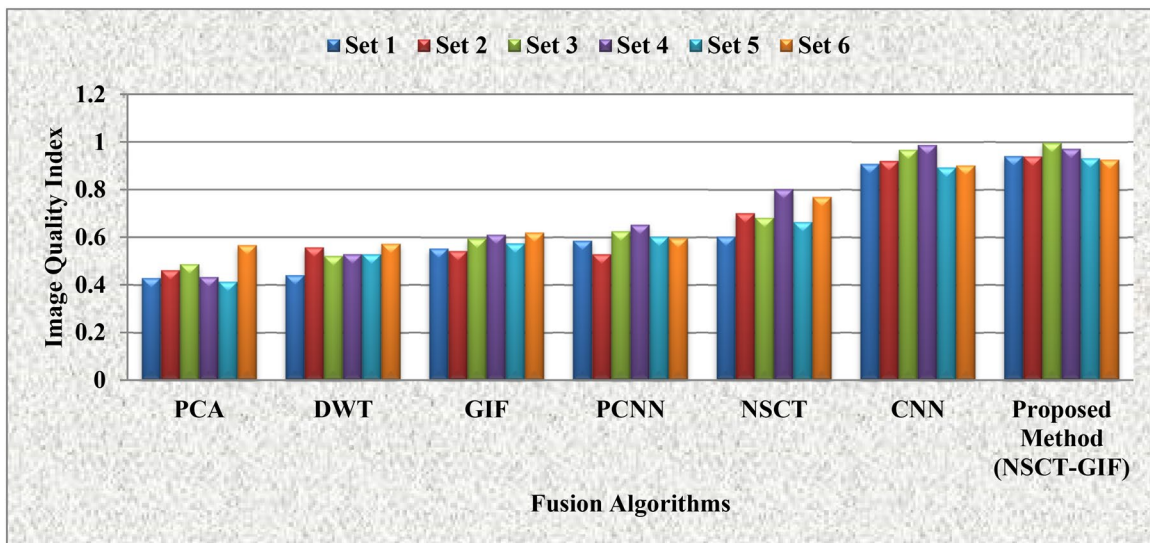**Fig. 8** Comparative analysis for fusion factor



**Fig. 9** Comparative analysis for Image Quality Index

The proposed method for hybrid fusion is contrasted to other traditional fusion methods, namely PCA, DWT, GIF, NSCT, PCNN, and CNN. All these strategies are applied as an average for estimated sub-band correlations and optimum value range for high-pass sub-band correlations, with fusion regulations. The proposed methodology is tested using analyzes of subjective and numerical parameters.

Figures 8 and 9 display the fusion component and IQI for the six CT-MRI, MRI-SPECT, and MRI-PET picture sets. The findings of the experiments are contrasted with the techniques PCA, DWT, GIF, PCNN, NSCT, and CNN. Compared with other current traditional methods, the proposed NSCT–GIF has higher fusion variable and IQI value.

Figures 10 and 11 demonstrate the comparable mSSIM and cross entropy analysis for the six CT-MRI, MRI-SPECT, and MRI-PET image collections. The outcomes of the experiments are contrasted with the techniques PCA, DWT, GIF, PCNN, NSCT, and CNN. The proposed NSCT-GIF has greater value for mSSIM and is given lower value for cross entropy relative to other traditional strategies that exist.

Figures 12 and 13 show the comparative study of CT-MRI, MRI-SPECT, and MRI-PET for the EQM and MI for the six set images. The outcomes of the experiments are contrasted with the strategies PCA, DWT, GIF, PCNN, NSCT, and CNN. Similar to the other current traditional methods,
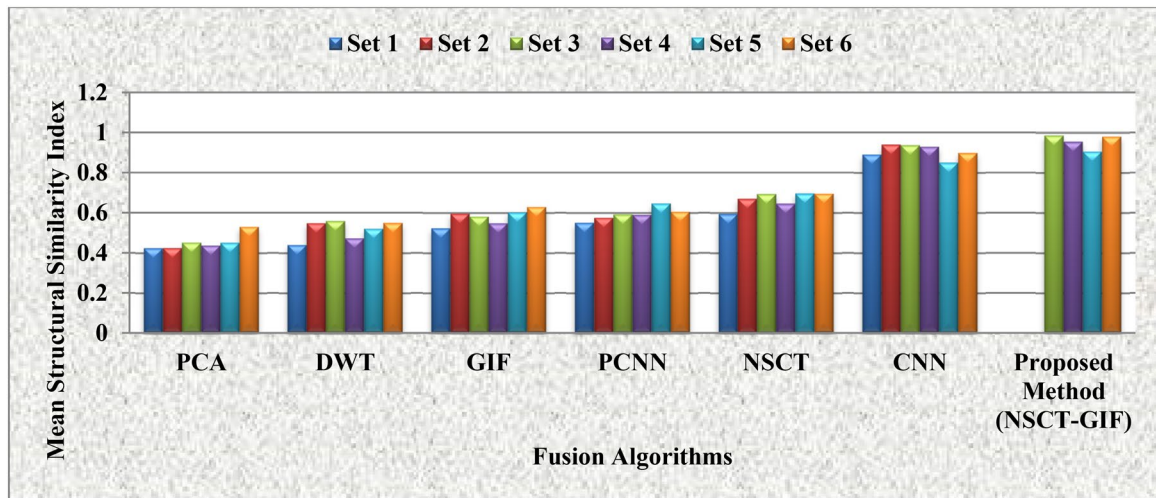
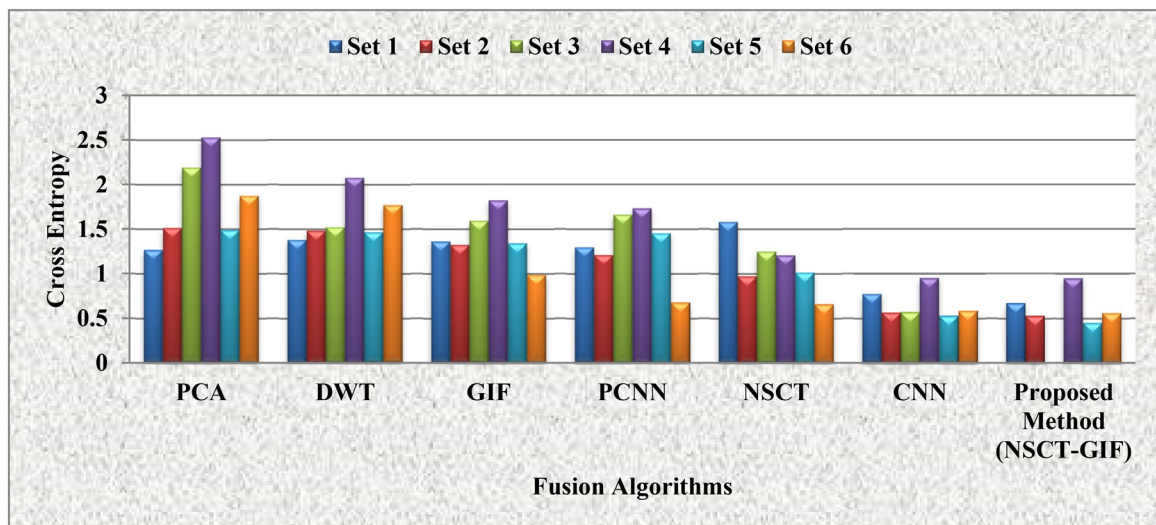**Fig. 10** Comparative analysis for mean structural similarity index



**Fig. 11** Comparative analysis for cross entropy

the proposed NSCT-GIF and PCNN-GIF have greater value for both EQM and MI.

Figures 14 and 15 demonstrate the PSNR detailed analysis and the standard deviation for six sets of CT-MRI, MRI-SPECT, and MRI-PET images. The findings of the experiments are contrasted with the methods PCA, DWT, GIF, PCNN, NSCT, and CNN. When compared with other current traditional methods, the proposed NSCT–GIF has higher value for PSNR and standard deviation.

## 5 Conclusions

This work examined the efficacy of various traditional methods, such as transform and neural network-guided filtering. Based on the convolutional neural networks, Siamese network is implemented to generate a direct mapping from input medical images to a weight map which contains the integrated pixel activity information and hybrid multimodal medical imaging fusion approaches using various assessment parameter values. The best medical imaging fusion
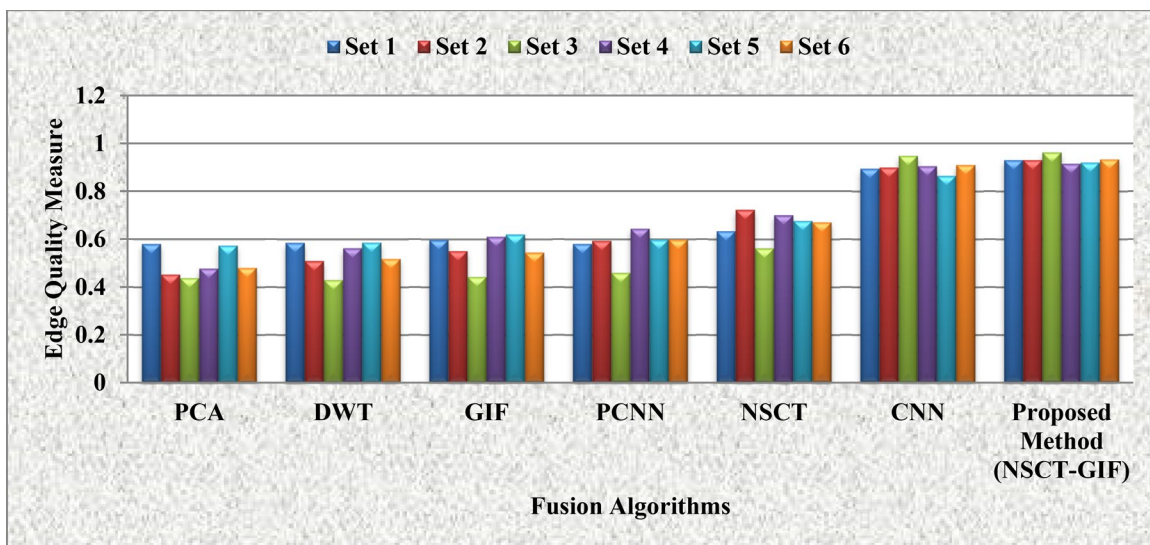
**Fig. 12** Comparative analysis for edge quality measure
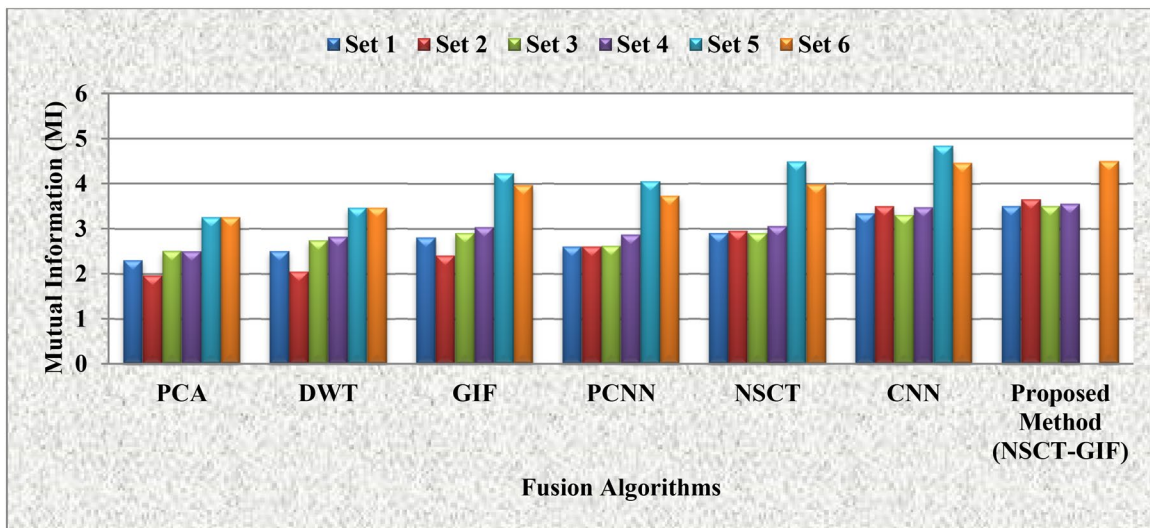


**Fig. 13** Comparative analysis for mutual information

approach has been applied using the latest hybrid methods. The suggested hybrid approaches (GIF-NSCT) have provided better results in all other traditional methods. It offers much more image details, better image quality, the fastest processing time, and better visual control. Both of these advantages make it a better selection for a variety of reasons for effective treatment, such as assisting with medical diagnosis. In addition to the proposed algorithm itself, another contribution of this work is that it exhibits greater potential of some deep learning techniques for image fusion, which will be further studied in the future.
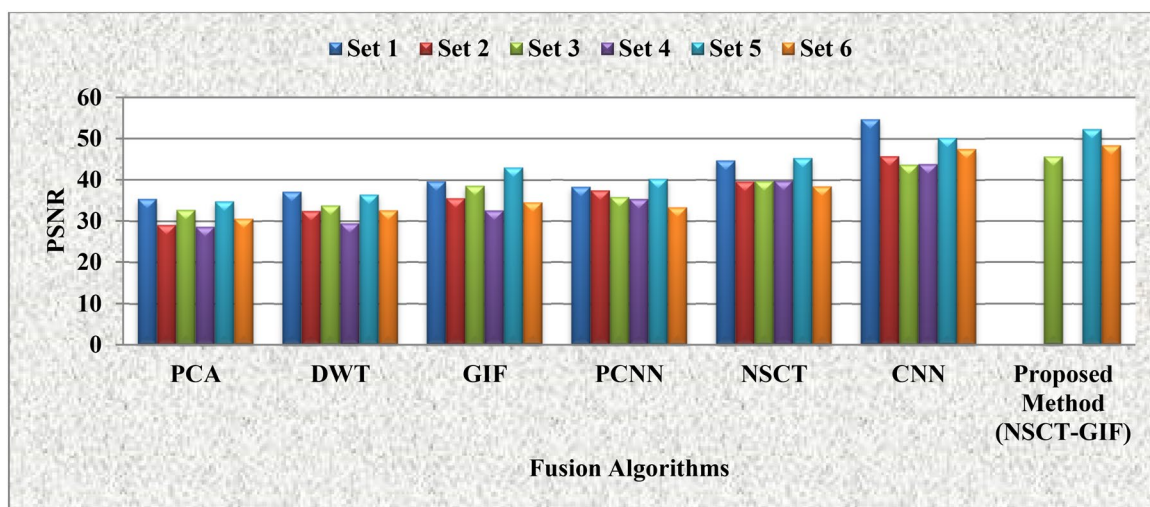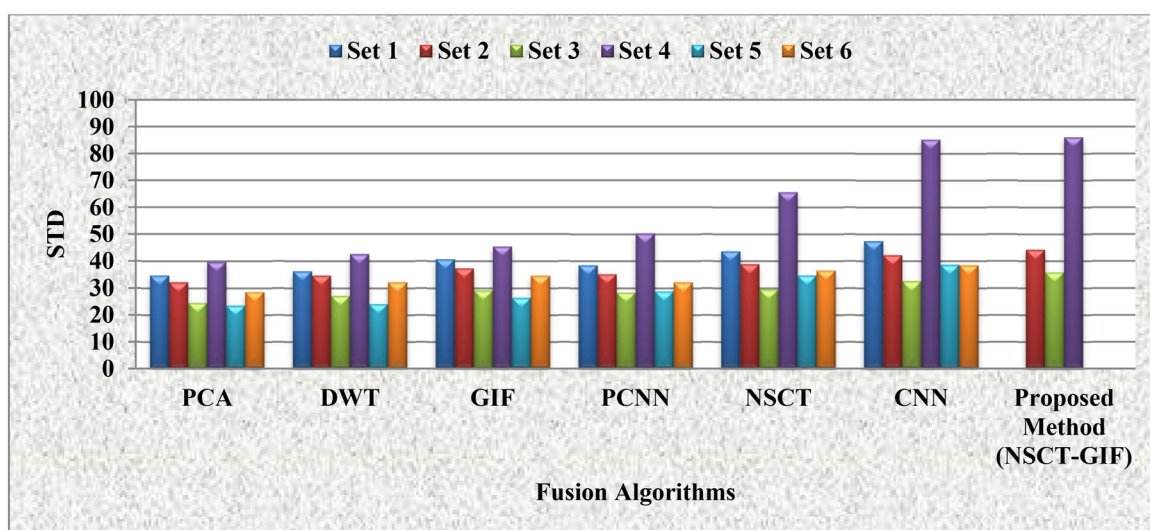
**Fig. 14** Comparative analysis for PSNR



**Fig. 15** Comparative analysis for standard deviation

# References

1. Stephan, T., Al-Turjman, F., Joseph, S., Balusamy, B.: Energy and spectrum aware unequal clustering with deep learning based primary user classification in cognitive radio sensor networks. Int. J. Mach. Learn. Cybern. (2020). https://doi.org/10.1007/s13042-020-01154-y

2. Ullah, F., Jabbar, S., Al-Turjman, F.: Programmers' de-anonymization using a hybrid approach of abstract syntax tree and deep learning. Technol. Forecast. Soc. Change **159**, 120186 (2020). https://doi.org/10.1016/j.techfore.2020.120186

3. Hossain, M.S., Amin, S.U., Muhammad, G., Al-Sulaiman, M.: Applying deep learning for epilepsy seizure detection and brain mapping visualization. ACM Trans. Multimedia Comput. Commun. Appl. **15**(1), 17 (2019)

4. Rajalingam, B., Priya, R.: Multimodal medical image fusion based on deep learning neural network for clinical treatment analysis. Int. J. ChemTech Res. **11**(06), 160–176 (2018)

5. Ramlal, S.D., Sachdeva, J., Ahuja, C.K., Khandelwal, N.: Multimodal medical image fusion using non-subsampled shearlet transform and pulse coupled neural network incorporated with morphological gradient. Signal Image Video Process. **12**, 1479–1487 (2018)

6. James, A.P., Dasarathy, B.V.: Medical image fusion: a survey of the state of the art. Inf. Fusion **19**, 4–19 (2014)

7. Gupta, D.: Nonsubsampled shearlet domain fusion techniques for CT-MR neurological images using improved biological inspired neural model. Biocybern. Biomed. Eng. **38**, 262–274 (2017)

8. Daniel, E.: Optimum wavelet based homomorphic medical image fusion using hybrid genetic—grey wolf optimization algorithm. IEEE Sens. J. **18**, 1558–1748 (2018)

9. Daniel, E., Anithaa, J., Kamaleshwaran, K.K., Rani, I.: Optimum spectrum mask based medical image fusion using Gray Wolf Optimization. Biomed. Signal Process. Control. **34**, 36–43 (2017)

10. Bhatnagar, G., Wua, Q.M.J., Liu, Z.: Human visual system inspired multi-modal medical image fusion framework. Expert Syst. Appl. **40**, 1708–1720 (2013)

11. Bhadauria, H.S., Dewal, M.L.: Medical image denoising using adaptive fusion of curvelet transform and total variation. Comput. Electr. Eng. **39**, 1451–1460 (2013)

12. Hermessi, H., Mourali, O., Zagrouba, E.: Convolutional neural network-based multimodal image fusion via similarity learning in the shearlet domain. Neural Comput. Appl. **30**, 2029–2045 (2018)

13. Shahdoosti, H.R., Mehrabi, A.: Multimodal image fusion using sparse representation classification in tetrolet domain. Digit. Signal Process. **79**, 9–22 (2018)

14. El-Hoseny, H.M., El-Rabaie, E.-S.M., Elrahman, W.A., El-Samie, F.A.A.: Medical image fusion techniques based on combined discrete transform domains. Arab Acad. Sci. Technol. Marit. Transp. IEEE, pp. 471–480 (2017)

15. Du, J., Li, W., Lu, K., Xiao, B.: An overview of multi-modal medical image fusion. Neurocomputing **215**, 3–20 (2016)

16. Jiao, Du., Li, W., Xiao, B., Nawaz, Q.: Union Laplacian pyramid with multiple features for medical image fusion. Neurocomputing **194**, 326–339 (2016)

17. Zonga, J.-J., Qiu, T.-S.: Medical image fusion based on sparse representation of classified image patches. Biomed. Signal Process. Control **34**, 195–205 (2017)

18. Xi, J., Chen, Y., Chen, A., Chen, Y.: Medical image fusion based on sparse representation and PCNN in NSCT domain. Comput. Math. Methods Med. (2018)

19. Tao, J., Li, S., Yang, B.: Multimodal image fusion algorithm using dual-tree complex wavelet transform and particle swarm optimization, CCIS 93, pp. 296–303. Springer, Berlin (2010)

20. Xia, K.J., Yin, H.S., Wang, J.Q.: A novel improved deep convolutional neural network model for medical image fusion. Cluster Comput. **22**, 1515–1527 (2018)

21. Chavan, S., Mahajan, A., Talbar, S.N., Desai, S., Thakur, M., D'cruz A, : Nonsubsampled rotated complex wavelet transform (NSRCxWT) for medical image fusion related to clinical aspects in neurocysticercosis. Comput. Biol. Med. **81**, 64–78 (2017)

22. Liu, Y., Chen, X., Cheng, J., Peng, H.: A medical image fusion method based on convolutional neural networks. In: 20th International Conference on Information Fusion, Xi'an, China—July 10–13 (2017)

23. Liu, Y., Chen, X., Peng, H., Wang, Z.: Multi-focus image fusion with a deep convolutional neural network. Inf. Fusion **36**, 191–207 (2017)

24. Liu, Y., Chen, X., Wang, Z., Wang, Z.J., Ward, R.K., Wang, X.: Deep learning for pixel-level image fusion: recent advances and future prospects. Inf. Fusion **42**, 158–173 (2018)

25. Du, C.B., Gao, S.S.: Multi-focus image fusion with the all convolutional neural network. Optoelectron. Lett. **14**(1), 71–75 (2018)

26. Sreeja, P., Hariharan, S.: An improved feature based image fusion technique for enhancement of liver lesions. Biocybern. Biomed. Eng. **38**, 611–623 (2018)

27. Xiaojun, Xu., Wang, Y., Chen, S.: Medical image fusion using discrete fractional wavelet transform. Biomed. Signal Process. Control **27**, 103–111 (2016)

28. Liu, X., Mei, W., Du, H.: Structure tensor and nonsubsampled sheasrlet transform based algorithm for CT and MRI image fusion. Neurocomputing **235**, 131–139 (2017)

29. Hossain, M.S., Muhammad, G.: Emotion recognition using deep learning approach from audio–visual emotional big data. Inf. Fusion. **49**(2019), 69–78 (2019)

30. Jacob, S., Menon, V., Al-Turjman, F., Mostarda, L.: Artificial muscle intelligence system with deep learning for post-stroke assistance and rehabilitation. IEEE Access **7**(1), 133463–133473 (2019)

31. Wang, J., Jabbar, S., Al-Turjman, F., Alazab, M.: Source code authorship attribution using hybrid approach of program dependence graph and deep learning model. IEEE Access **7**(1), 141987–141999 (2019)